Titanium dioxide aggregating nanoparticles induce autophagy and under-expression of microRNA 21 and 30a in A549 cell line: A comparative study with cobalt(II, III) oxide nanoparticles

Toxicology in Vitro xxx (2017) xxx-xxx

Contents lists available at ScienceDirect

Toxicology in Vitro

journal homepage: www.elsevier.com

Titanium dioxide aggregating nanoparticles induce autophagy and under-expression of microRNA 21 and 30a in A549 cell line: A comparative study with cobalt(II, III) oxide nanoparticles

Rossella Alinovi[a, 1], Matteo Goldoni[a, *], Silvana Pinelli[a, 1], Francesca Ravanetti[b], Maricla Galetti[c], Giorgio Pelosi[d, 1], Giuseppe De Palma[e], Pietro Apostoli[e], Antonio Cacchioli[b], Paola Mozzoni[a], Antonio Mutti[a]

[a] Department of Medicine and Surgery, University of Parma, Parma, Italy
[b] Department of Medical Veterinary Sciences, Unit of Normal Veterinary Anatomy, University of Parma, Parma, Italy
[c] Italian Workers' Compensation Authority (INAIL) Research Center, Parma, Italy
[d] Department of Chemistry, Life Sciences and Environmental Sustainability, University of Parma, Parma, Italy
[e] Section of Public Health and Human Sciences, Department of Medical and Surgical Specialties, Radiological Sciences, and Public Health, University of Brescia, Brescia, Italy

ARTICLE INFO

Keywords:
TiO_2
Co_3O_4
Nanoparticles
Autophagy
microRNA
Oxidative stress

ABSTRACT

The toxicity of TiO_2 nanoparticles (NPs) is controversial, while it is widely accepted for Co_3O_4 NPs. We present a comparative study concerning the uptake of these NPs and their effect on cytoplasmic organelles and autophagy in a human lung carcinoma cell line (A549), including assays on the expression of autophagy-related microRNAs. The NP accumulation caused a fast dose- and time-dependent change of flow cytometry physical parameters particularly after TiO_2 NP exposure. The intracellular levels of metals confirmed it, but the Co concentration was ten times higher than that of Ti. Both NPs caused neither necrosis nor apoptosis, but cytotoxicity was mainly evident for Co_3O_4 NPs in the first 72 h. TiO_2 NPs caused autophagy, contrarily to Co_3O_4 NPs. Furthermore, a significant and persistent downregulation of miRNA-21 and miRNA-30a was observed only in TiO_2 NPs-treated cultures. The expression of miRNA-155 was similar for both NPs. Oxidative stress was evident only for Co_3O_4 NPs, while both NPs perturbed endoplasmic reticulum and p-53 expression. In conclusion, the oxidative stress caused by Co_3O_4 NPs can influence energy homeostasis and hamper the ability to detoxify and to repair the resulting damage, thus preventing the induction of autophagy, while TiO_2 NPs elicit autophagy also under sub-toxic conditions.

1. Introduction

Nano-sized TiO_2 is used in a wide range of applications, mainly due to its ability to confer whiteness and opacity onto various products (e.g. paints, papers and cosmetics) and to its light-scattering properties and very high refractive index (EPA, 2009). Over the last few years, the potential hazard of TiO_2 nanoparticles (NPs) has been debated and questioned (Skocaj et al., 2011). There is evidence that respirable TiO_2 particles may persist in the lung of exposed workers some years after the end of exposure with local macrophagic responses and mild fibrosis (NIOSH, 2011). Furthermore, a small but significant increase in lung cancer mortality among exposed workers was found (Boffetta et al., 2004). Based on experimental data, IARC has classified generically TiO_2 as a Group 2B carcinogen (possibly carcinogenic to humans) by inhalation (IARC, 2010). On the other hand, NIOSH concluded that there is insufficient evidence to classify TiO_2 in any form as a potential occupational carcinogen (NIOSH, 2011).

Several animal studies have shown that TiO_2 NPs cause chronic inflammation and lung tissue damage, which can lead to lung-tumor de-

Abbreviations: 3MA, 3-methyl adenine; BCA, bicinchoninic acid; DCFH-DA, 2′,7′-dichlorodihydrofluorescein diacetate; ELISA, enzyme-linked immunosorbent assay; ER, endoplasmic reticulum; FBS, Fetal bovine serum; GRP78, Glucose-regulated protein; ICP-MS, Inductively coupled plasma mass spectrometry; miRNA, microRNA; NP, Nanoparticle; PBS, Phosphate buffer solution; ROS, Reactive oxygen species; RT-PCR, Reverse transcription-polymerase chain reaction; SEM, scanning electron microscope; SSC, Side-scattered light; TBARS, Thiobarbituric Acid Reactive Substances; TEM, transmission electron microscope.

* Corresponding author at: Department of Medicine and Surgery, University of Parma, Via Gramsci 14, 43126 Parma, Italy.
Email address: matteo.goldoni@unipr.it (M. Goldoni)
[1] C.I.R.C.M.S.B. (Consorzio Interuniversitario di Ricerca in Chimica dei Metalli nei Sistemi Biologici), Parma Unit, University of Parma, Parma, Italy.

http://dx.doi.org/10.1016/j.tiv.2017.04.007
Received 23 December 2016; Received in revised form 14 March 2017; Accepted 7 April 2017
Available online xxx
0887-2333/

velopment (Lindberg et al., 2012; Sager et al., 2008; Sycheva et al., 2011). Furthermore, TiO_2 NPs induce dose-dependent hyperplasia, inflammation, but also disruption or dysfunction of endoplasmic reticulum (ER) and mitochondria, leading to abnormal autophagy (Yu et al., 2015b). Other studies in the literature report in vivo and in vitro effects of TiO_2 NPs (Han et al., 2013; Kenzaoui et al., 2012; Montiel-Davalos et al., 2012), but in many cases no cytotoxic effects were observed (Moschini et al., 2013; Prasad et al., 2013; Shi et al., 2013; Zhang et al., 2015). The mechanisms underlying TiO_2 NPs toxic responses are not clear, although oxidative stress and DNA damage induction may be responsible for adverse biological effects (Skocaj et al., 2011). Considering A549 as a model of epithelial pulmonary cells, previous studies have reported the genotoxic and cytotoxic effects of TiO_2 NPs (Jugan et al., 2012; Karlsson et al., 2008; Srivastava et al., 2013; Ursini et al., 2014).

For a better comprehension of the mechanisms underlining pulmonary toxicity of TiO_2 NPs, we used the A549 cells focusing on the uptake and metabolic responses/adaptation to the internalized NPs, looking at the cytoplasmic organelles perturbation and autophagic process. Different NPs may induce autophagy, so that they are considered to be a new class of autophagy activators (Chatterjee et al., 2014; Stern et al., 2012).

In this study we compare TiO_2 with Co_3O_4 NPs. Co_3O_4 NPs have been increasingly used in biomedical applications, orthopaedics, electronics, energy storage, electrochemistry, pigments, etc. for their unique magnetic, size- and shape-dependent properties. Presently they are raising concerns about their potential health effects and risk in occupational environment (Alarifi et al., 2013; Colognato et al., 2008; Horev-Azaria et al., 2011; Papis et al., 2009). This comparison is particularly interesting for two main reasons: (1) their extensive production and widespread use, potential workplace exposure, commercial availability and existing information on such materials; (2) the need to gather information about specific targets (heart, lung, bowel, skin), with existing recent data about in vitro effects (Alinovi et al., 2015; Cavallo et al., 2015; Crosera et al., 2015; Larese Filon et al., 2013; Spigoni et al., 2015; Titma et al., 2016; Ursini et al., 2014).

Finally, we have explored the relationship between autophagy and microRNAs (miRNAs) which is poorly studied in literature with NPs. MiRNAs are endogenous short non-coding RNAs able to regulate gene expression at post-transcriptional and translational levels via complementary base-pairing with mRNA. MiRNAs play a critical role in a broad range of biological processes including proliferation, differentiation, apoptosis and stress response. Single miRNAs can simultaneously regulate a multitude of targets and biological networks. Autophagy is post-transcriptionally regulated by small non-coding miRNAs and can be crucial in tumorigenesis (Frankel and Lund, 2012; Yao et al., 2016). For this reason, our study has been focused on autophagy including the evaluation of some miRNAs controlling different functions and mechanisms.

2. Materials and methods

2.1. Reagents

Sterile plastic material for cell culture was purchased from Costar, Corning (Amsterdam, The Netherlands). ApoTox-Glo™ Triplex Assay, CytoTox-One™ Homogeneous Membrane Integrity Assay, CellTiter-Glo® Luminescent Cell viability Assay were obtained from Promega (Madison, WI, USA) and Annexin V/FITC kit Assay from Bender MedSystems GmbH (Vienna, Austria). DCFH-DA was provided from Molecular Probes (Eugene, OR, USA), GSH colorimetric kit and Cyto-ID® Autophagy Detection kit from Enzo Life Sciences International Inc. (Plymouth Meeting, PA, USA), BCA Protein Assay from Thermo Scientific (Rockford, IL, USA). FITC mouse anti-human p53 antibody was purchased from Dako Italia s.r.l. (Milan, Italy), along with their respective isotype controls. Cobalt (II,III) oxide nanopowder (< 50 nm) and TiO_2 nanopowder (< 100 nm) are commercially available and were provided with physicochemical characterization by Sigma (St. Louis, MO, USA). All other reagents were from Sigma (St. Louis, MO, USA), unless otherwise specified.

2.2. Characterization of TiO_2 and Co_3O_4 NPs

The characterization of NPs has been already published (Alinovi et al., 2015). Briefly, Co_3O_4 NPs had an irregular non spherical shape, forming agglomerates of tens of NPs in water. Size distribution was centered around a mean value of 17 nm (diameter). TiO_2 NPs had a regular spherical shape and were slightly aggregated, with a wide size distribution centered around a value of 38 nm. Mean surface areas of TiO_2 and Co_3O_4 NPs were respectively 13.8 m^2/g and 46.7 m^2/g. In culture media, TiO_2 NPs tended to form larger clusters than in water. The contrary was observed for Co_3O_4 NPs. TiO_2 NPs had lower zeta potential than Co_3O_4 NPs in water (− 31.7 vs. − 19.1 mV), with similar values in culture media.

2.3. Preparation of NPs

Co_3O_4 and TiO_2 NPs were prepared as already reported (Alinovi et al., 2015).

2.4. Ti and Co determination

Intracellular total Ti and Co concentrations were determined after 24 h-exposure. A549 were washed three times with PBS, harvested, pelleted and digested in 30% nitric acid overnight at 65 °C, then analyzed by means of ICP-MS (Elmer ELAN DRC II instrument Perkin Elmer Sciex, Woodbridge, ON, Canada). The limit of detection (LOD) was 0.1 μg/l. Metal concentrations were referred to the cell number and expressed as ng per 10^6 cells. Regarding the solubility, NPs at 20–50–100 μg/ml were left 24 h the culture medium at 37 °C. After centrifugation (12,000*g* ∗ 10 min), the supernatant was collected and Co-Ti were measured by means of ICP-MS. The intra-sample variability was always < 3%. Regarding Co dissolution, cells were exposed for 24 h to the supernatant of NPs after centrifugation (12,000*g* ∗ 10 min) and to 50 μg/ml NPs. Then, A549 were harvested, pelleted, re-suspended in 1000 μl of water, freeze/thawed three times, sonicated and finally centrifuged (12,000*g* ∗ 10 min). The supernatant was used to measure intracellular ionic Co.

2.5. Adsorption of serum proteins on NPs

The coating "corona" was analyzed by incubation NPs with FBS or complete medium containing 10% FBS. NPs were normalized for the total particle surface (0.08 m^2) and incubated with 500 μl FBS, or medium or water, at 37 °C for 30 min. Afterward, samples were purified by 5 cycles of centrifugation (16,000*g*) and the pellet was dispersed in water to remove unabsorbed proteins. NPs were then re-suspended overnight in 100 μl reducing loading buffer, centrifuged and the supernatants were heated to 95° for 10 min. A 1:100 dilution of FBS in purified water was used as a positive control. Identical volumes (50 μl) of supernatants, as well as the protein markers and the diluted FBS, were applied on 10% polyacrylamide gel prepared on a Mini-Protean Electrophoresis System (Bio-Rad, Hercules, CA, USA) and ran at constant voltage. The protein bands were stained with Coomassie Blue, processed by Fluor-S Multi-Imager and analyzed by Quantity-One software (Bio-Rad, Hercules, CA, USA).

2.6. Cell culture

A549 cells were cultured in RPMI 1640 medium supplemented with 10% heat-inactivated FBS, 100 U penicillin ml^{-1} and 100 μg streptomycin ml^{-1}, 2 μM L-glutamine and incubated at 37 °C with humidified air containing 5% CO_2. Exponentially growing cells were used for all assays.

2.7. SEM morphological analysis

For SEM analysis NPs treated and control cells were fixed at with 2.5% glutaraldehyde in 0.1 M sodium cacodylate buffer (pH 7.3). They were then dehydrated through a series of alcohols and then critical-point-dried with liquid CO_2 (CPD 030 Baltec). Specimens were then sputter-coated with a gold–palladium layer using a SCD 040 coating device (Balzer Union) (Ravanetti et al., 2010). Samples were observed using a Zeiss DSM 950 scanning electron microscope at an accelerating voltage of 10 kV (Zeiss).

2.8. TEM ultrastructural analysis

NPs treated and control cell fixed in 2.5% glutaraldehyde/0.1 M PBS buffer pH 7.2 for 1 h and then dehydrated through the graded series of acetone and embedded in Durcupan (Fluka Chemie, Buchs, Switzerland). The polymerization occurred after 24 h at 65 °C. Sections of 2 μm were prepared using ultramicrotome Reichert (Pabisch-Wien, Austria), colored with Toluidin blue 0.5% sodium carbonate, and observed under a light microscope. Ultrathin sections (~ 70 nm) were cut with a diamond blade, gathered on slotted copper grills, stained with 3% uranyl acetate and lead citrate 6 (Cacchioli et al., 2014) and observed by a JEOL (JEM 2200 FS, Tokyo, Japan)) transmission electron microscope operated at 80 keV.

2.9. Cell proliferation/viability assays

Viability and cytotoxicity of A549 cells treated with NPs were determined by three different assays: ApoTox-Glo™ Triplex Assay, CytoTox-One™ Homogeneous Membrane Integrity Assay and CellTiter-Glo Luminescent Cell Viability Assay, following the manufacturer's instructions. Luminescence/fluorescence was detected by a Cary Eclipse fluorescence spectrophotometer (Varian, Inc., Palo Alto, CA, USA) and the data were normalized against control values. Cell number was also evaluated by cell counting in a Burker hemocytometer. Experiments with TiO_2 NPs were repeated after pre-treatment of cells with 5 mM 3-methyl adenine (3MA) as autophagy blocker.

2.10. Clonogenic survival assay

Exponentially growing A549 cells were diluted to have an appropriate plating density, seeded in 6-well plates and allowed to adhere overnight. After addition of increasing concentrations of NPs, cells were cultured for 10 days. Colonies were fixed with methanol/acetic acid (3:1) and stained with crystal violet (0.5% w/v in methanol). Colonies consisting of 50 cells or more were counted using the Fluor-S MultiImager (Bio-Rad, Hercules, CA, USA). The surviving fraction was calculated relative to the mean plating efficiency of untreated control cells. Experiments with TiO_2 NPs were repeated after pre-treatment of cells with 5 mM 3MA.

2.11. Apoptosis assays

Apoptosis was evaluated by phosphatidylserine translocation from the inner to the outer leaflet of the membrane and by caspase-3 activation, as already described (Alinovi et al., 2015.

2.12. Flow cytometric analysis

A FC500™ flow cytometer (Instrumentation Laboratory, Bedford, MA, USA) was used in this study. The analysis was performed using the FlowJo software package (Tree Star Inc., Ashland, OR, U.S.A.). The mean of SSC values was calculated, referred to the SSC mean of control samples (treated/control) and represented as the "mean SSC ratio".

2.13. Autophagy

Autophagic cells were stained by Cyto-ID Green Detection Reagent for 30 min, according to manufacturer's protocol. For flow cytometry after 24 h treatment with NPs, cell suspensions were incubated with the probe before the analysis. Cells grown on glasses were exposed to NPs for 24 h, then incubated with Cyto-ID Green Detection Reagent before fixation with 4% paraformaldehyde for 20 min. Finally, the nuclear dye DRAQ5® (Cell Signaling Technologies, Danvers, MA, USA) was applied to slides. The confocal system was the LSM 510 Meta scan head integrated with the Axiovert 200 M inverted microscope (Carl Zeiss, Jena, Germany). Specimens were observed through a 63 ×, /1.30 oil objective The green-emitting fluorescent probe to highlight the vacuolar components of the autophagy pathway and the nuclear dye were excited with 488 nm argon and 633 nm He-Ne laser lines, respectively. Image acquisition was carried out in a multitrack mode through consecutive and independent optical pathways. A series of x-y sections was acquired with a z-step of 0.5 μm, to cover the whole height of the samples.

2.14. Oxidative stress

Intracellular ROS levels were quantified by flow cytometer using 2′,7′-dichlorodihydrofluorescein diacetate (DCFH-DA) (Alinovi et al., 2015).

The well-established method 'Thiobarbituric Acid Reactive Substances' (TBARS) allowed to monitoring lipid peroxidation, as already described (Alinovi et al., 2015), using a Cary Eclipse fluorescence spectrophotometer (Varian, Inc., Palo Alto, CA, USA) (excitation 515 nm, emission 545 nm). All values were normalized for the protein concentrations and expressed as percentage of control. Experiments with TiO_2 NPs were repeated after pre-treatment of cells with 5 mM 3MA.

2.15. p53 expression

After treatment with NPs for 4, 8, 12, and 24 h, A549 cells were resuspended in PerFix assay kit (Beckman Coulter) for 15 min at RT, according with the manufacturer's instructions, before the incubation with the mouse anti-human p53-FITC antibody for 30 min in the dark. Labeled cells were sorted by flow cytometer.

2.16. GRP78 enzyme-linked immunosorbent assay

Glucose-regulated protein (GRP78) or binding immunoglobulin protein (BiP), was quantified in lysates of treated and control cells using a commercially available competitive enzyme-linked immunosorbent assay (ELISA), according with the manufacturer's instructions. All values were referred to protein concentrations.

2.17. Protein determination

In cellular lysates total protein concentrations were quantified by the BCA (bicinchoninic acid) Protein Assay, according to the manufacturer's microwell plate protocol.

2.18. Total RNA isolation

RNA was isolated from cultured cells using TRIzol reagent (Thermo Fisher Scientific, MA USA) according to the manufacturer's instructions. The extracted RNA was digested with DNase I (DNA-free kit; Thermo Fisher Scientific, MA USA) to remove any genomic DNA contamination. Total RNA was quantified using a NanoDrop spectrophotometer (Thermo Scientific, DE).

2.19. Reverse transcription and quantification of miRNA expression by qRT-PCR

Total RNA was reverse transcribed using a TaqMan MicroRNA RT kit (Thermo Fisher Scientific, MA USA) according to the manufacturer's instruction. The reaction included 3 μl of stem-loop RT primer 50 nM, 1.5 μl of 10 × RT buffer, 0.15 μl of dNTPs 100 mM, 0.19 μl RNase Inhibitor 20 U/μl, 1 μl of MultiScribe reverse transcriptase 50 U/μl and 5 μl of RNA sample in a total volume of 15 μl. Quantitative PCR was performed using an iCycler iQ Real-Time Detection System (Bio-Rad, Hercules, CA). The reaction consisted of one step at 95 °C for 10 min, followed by 40 cycles of 95 °C for 15 s and 60 °C for 1 min. All of the assays were made in duplicate, and one no-template and two interpolate controls were used in each experiment. The expression of the miRNAs was calculated using the comparative cycle threshold (Ct) method. The threshold cycle (Ct) was defined as the fractional cycle number at which the fluorescence passed the fixed threshold. The Ct values of the target miRNAs were normalized to sno-RNU6B and the fold-change in expression of each miRNA were calculated using the equation $2^{-\Delta\Delta Ct}$ (Livak and Schmittgen, 2001). Experiments with TiO_2 NPs (24 h-exposure) were repeated after pre-treatment of cells with 5 mM 3MA.

2.20. Statistical analysis

Data were expressed as mean ± SD (standard deviation) of at least three independent experiments (at least five replicates for each experiment). One-way ANOVA followed by Dunnett post-hoc test was performed to detect the differences among different culture conditions. Statistical significance was set at $p < 0.05$ (two-sided). Data analysis was performed using SPSS version 20.0 (SPSS Inc./IBM, Chicago, Ill, USA).

3. Results

The results concerning the protein corona are shown in Supplementary material (Fig. S1A). The diluted FBS showed mainly one protein band according to the molecular weight of albumin (67 kDa). By comparing the results of the two different NP preparation, protein bands clearly revealed a higher amount of corona proteins on TiO_2 NPs [6.92 ± 0.94 higher than Co_3O_4 NPs]. For both NPs, pre-incubation with medium containing 10% FBS caused an almost "saturation" effect. The corona-originated protein profiles for both NPs had similar molecular weight distributions, where the medium-sized proteins (30–100 kDa) were predominant (Fig. S1B and Table S1).

3.1. Cellular uptake

The percent of solubility of NPs was not concentration-dependent in the range 10-100 μg/ml (Fig. S2) and overall it was 0.78 (SD: 0.08) % for Co_3O_4 NPs and 2.21 (SD: 0.07) % for TiO_2 NPs. The concentration of dissolved Co in culture medium + FBS at 50 μg/ml was 280 (SD: 27) μg/l (4.75 μM) and that of Ti was 840 (SD: 60) μg/l (17.5 μM).

Regarding Co_3O_4 NPs, single NP or small groups of NPs were absorbed by the cell membrane via macro pinocytosis. Small endosomes typified the first step of the internalization process. Regarding TiO_2 NPs, the internalization usually occurred for clusters of NPs of some hundreds nm in diameter. Different types of cytoplasmic vesicles were observed; as for Co_3O_4 NPs, endosomes typified the first step of the internalization process, thereafter NPs were compartmentalized into round big vesicles in the cytoplasm. Evidence of the presence of autophagosome was detected only for TiO_2 NPs (Fig. 1A–B).

The intracellular NP accumulation caused a dose- and time-dependent modification of physical parameters. The cytogram distribution, for instance, increased in SSC intensity (Fig. 2A–B). These changes in SSC distributions were dramatically evident for TiO_2 NPs starting from 30 min after the beginning of exposure. Inhibition of type III Phosphatidylinositol 3-kinases (PI-K3) by incubation with 3MA completely blocked these self-degradative processes and significantly reduced SSC changes (Fig. 2B). The mean SSC ratio over 24 h of A549 treated with NPs is shown in Fig. 2C. For both NPs, this increase was very fast and reached a plateau for the following 4 h. There was a 3.7-fold increase in SSC between 20 μg/ml and control for Co_3O_4 NPs and a 24.4-fold increase for TiO_2 NPs after 4 h. The intracellular levels of the metals confirmed a dose-dependent adsorption, but the intracellular Co concentration was ten time higher than that of Ti (Fig. 2D). The overall amount of internalized Co_3O_4 NPs was about 1/6 of the initial one, about 1/60 for TiO_2 NPs. When cells were exposed only to the supernatant, the intracellular soluble Co concentration was 3.3 (SD: 0.1) ng/10^6 cells, while was 23.6 (SD: 3.5) ng/10^6 cells after 24 h–NP exposure at 50 μg/ml subtracting the fraction of soluble Co spontaneously released by NPs during the preparation of samples. No cytotoxic effects of Co ions were observed until to 100 μM (data not shown).

3.2. Cellular viability and proliferation

From the analysis carried out through the scanning electron microscopy, no alterations in cell morphology between cells treated with Co_3O_4 and TiO_2 NPs and their controls were detected. As shown in Fig. S3, in all the tested conditions cells displayed a healthy heterogeneous morphology; round, polygonal or bipolar morphology and spread and flattened cells were detected. In the concentration range used in the test (1–100 μg/ml) A549 presented different patterns of response to Co_3O_4 and TiO_2 NPs (Fig. S4). Both NPs did not cause necrosis, evaluated by LDH spontaneous release of LDH in the medium (not shown), but in cultures of A549 exposed to Co_3O_4 NPs, significant decreases in the cell number and of intracellular ATP started from 24 h and continued after 72 h. The same was not observed during TiO_2 NPs treatment, except for a significant reduction in the number of cells after 72 h. The pre-treatment with 3-MA induced a significant decrease in cell number after 24 h of exposure at TiO_2 NPs concentration of 50 and 100 μg/ml, with no significant later effects (Fig. S5).

Caspase-3 activation and phosphatidylserine translocation were evaluated after 24 h, but no significant activation and no apoptosis were observed (Fig. S6).

The long-term effects of NPs on cell survival were assessed by clonogenic assay. The persistent presence of both NPs resulted in a sig-

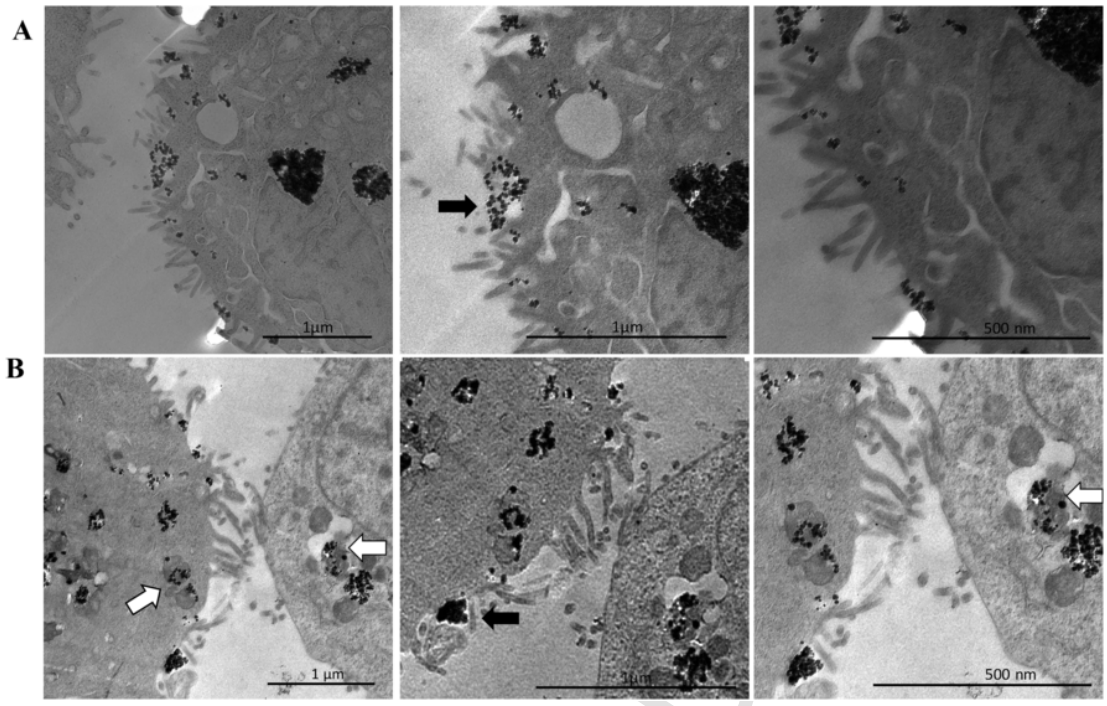

Fig. 1. TEM micrographs of NPs internalization. (A) Co_3O_4 NPs. Black arrow = small NP aggregates.(B) TiO_2 NPs. Different types of cytoplasmic vesicles are observed. Evidence of autophagosome (white arrows).

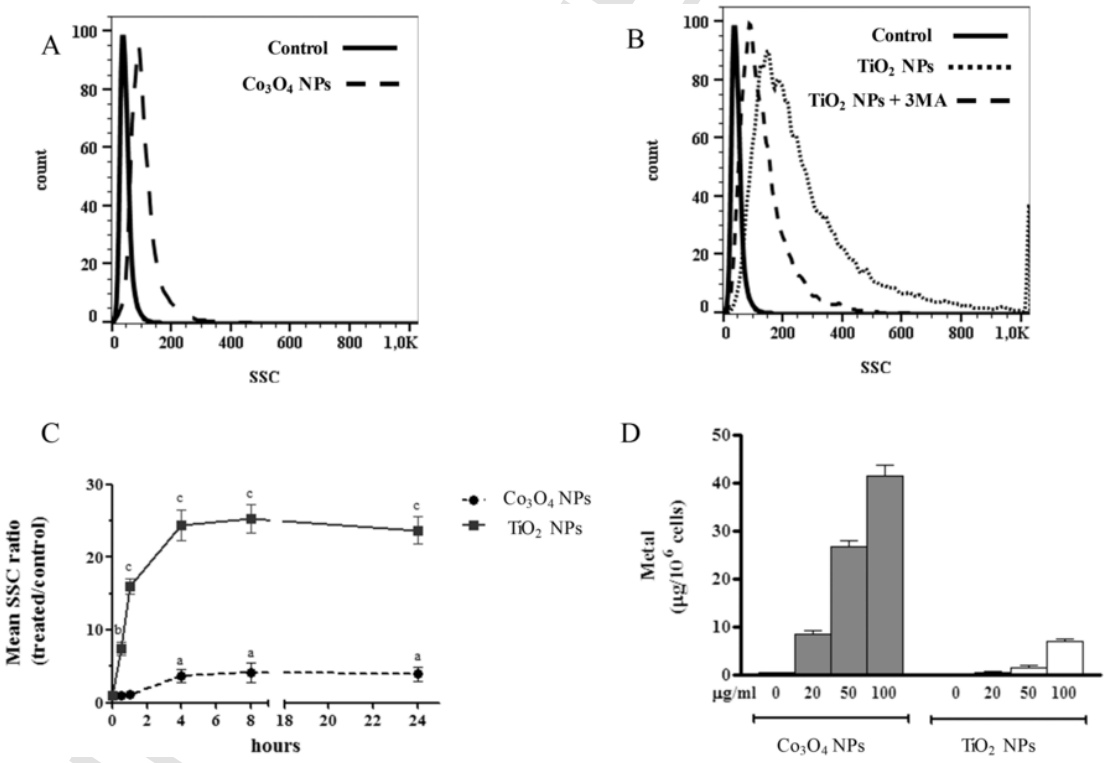

Fig. 2. Cellular uptake. (A) and (B) flow-cytometry analysis of side scatter (SSC) in A549 cells. Unexposed cells were scanned as control (continuous line) and compared to cells exposed to NPs for 4 h (dashed line). (C) SSC was measured over a 24 h period [NPs = 50 µg/ml]. (D) Evaluation of intracellular Co and Ti in A549 cells treated for 24 h with different concentration of NPs. Results are shown as means ± SD. Significant differences from controls: [a]:$p < 0.05$; [b]:$p < 0.01$; [c]:$p < 0.001$.

nificant decrease of clonogenic activity (Fig. S7), while the removal of NPs after a 24 h pretreatment restored the plating efficiency and the cell survival (not shown).

3.3. Autophagy

The changes in cellular parameter SSC during treatment with TiO2 NPs was further explored considering the autophagy pathway. No ev-

idence of autophagy activity was detected during exposure to Co_3O_4 NPs (Fig. 3A and C). On the contrary, TiO_2 NPs caused a significant increase of autophagosomes as assessed by flow cytometry (increase 49,2 ± 5,3% of mean fluorescence at 20 μg/ml as compared to control, Fig. 3B–C) confirming microscopy observations (a clear difference in cytoplasmic dye, Fig. 4). The presence of multiple autophagic vesicles containing NPs was observed only in the TiO_2 NPs treated samples.

The expression of miRNA-30a and miRNA-21 in cells exposed to NPs was also tested. A significant and persistent downregulation of these autophagy-related miRNAs in TiO_2 NPs treated cultures was observed, although this response occurred at different times and to a different extent. During Co_3O_4 NPs treatments decreases were lower and temporary (Fig. 5A-B), with a recovery at 24 h for miRNA-21 and an upregulation for miRNA-30a. Pre-treatment of cells with 3-MA suppressed downregulation at 24 h due to TiO_2 (Fig. S8). On the other hand, the expression of miRNA-155 is similar for both NPs. An increase was observed after 2 h (2–4 h for Co_3O_4 NPs) with a subsequent decrease at longer times of exposure (Fig. 5C).

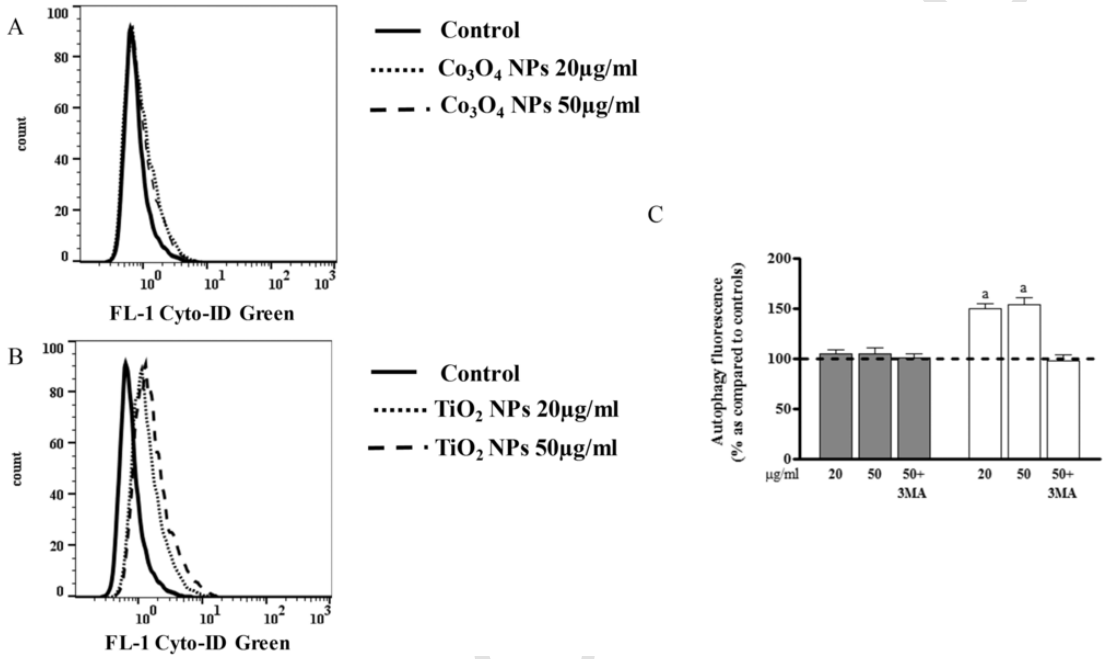

Fig. 3. Flow cytometry-based analysis of autophagy induction in A549 cells treated with Co_3O_4 (A) and TiO_2 NPs (B) for 24 h. Results are presented as histogram overlay. (C) Quantitative results. Grey bars: Co_3O_4 NPs at 20, 50 and 50 + 3-MA μg/ml. White bars: the same for TiO_2 NPs. Significantly different from untreated control: [a]: $p < 0.05$; [b]: $p < 0.01$; [c]: $p < 0.001$.

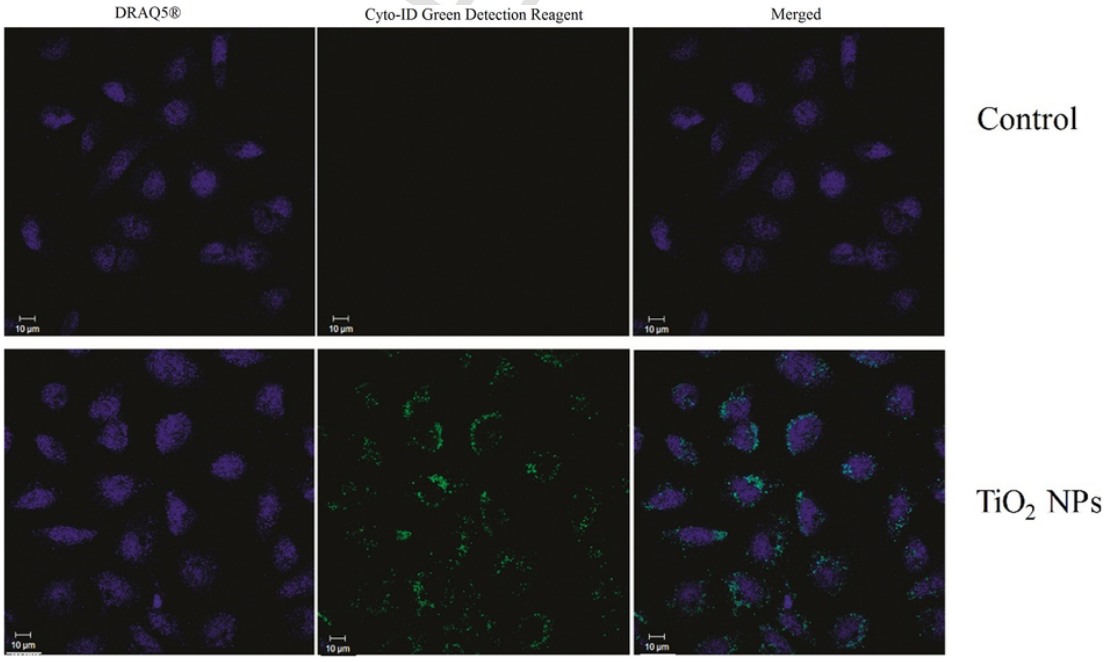

Fig. 4. Morphological phenomena of autophagy in TiO_2 NPs-treated lung cancer cells (50 μg/ml for 24 h) looking at nuclear dye, cytoplasm dye and merged imagine. Samples stained with autophagy probe were examined under confocal microscope.

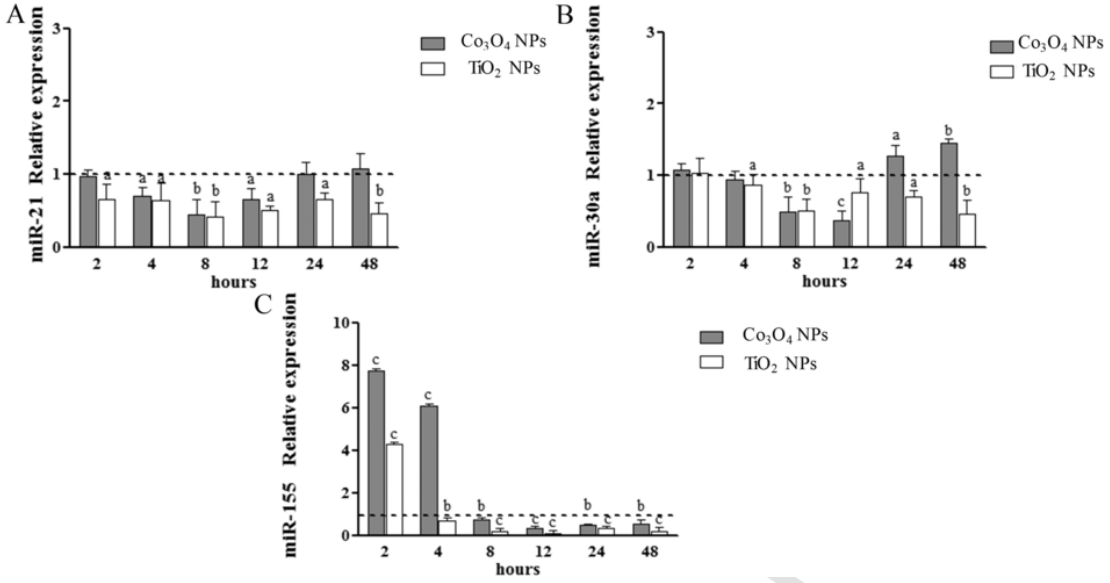

Fig. 5. Relative expression changes of miRNA-21, miRNA-30a miRNA-155 (vs. untreated controls) in human A549 cells during NPs exposure. Significantly different from control: [a]: $p < 0.05$; [b]: $p < 0.01$; [c]: $p < 0.001$.

3.4. Cellular function/activity

Co_3O_4 NPs induced intracellular ROS generation, reaching a highly significant increase after 30 min (Fig. 6A). ROS production was accompanied by an increase of lipid peroxidation (TBARS), protein oxidation and induction of HO-1 expression after 24 h–exposure. TiO_2 NPs showed only a significant effect on TBARS at 24 h–exposure, with no effects of a pre-treatment with 3-MA (not shown).

Finally, GRP78 concentration significantly increased in cells treated with both NPs than in the controls (Fig. 6B). At the same time-points the intracellular levels of p53 were enhanced for both NPs (Fig. 6C).

4. Discussion

Very high concentrations of TiO_2 NPs have few cytotoxic effects on endothelial cells, whereas Co_3O_4 NPs impair cell metabolism in a concentration- and time-dependent manner and induce oxidative stress, without evident cellular death or apoptosis induction (Alinovi et al., 2015). However, both NPs significantly induced expression of adhesion

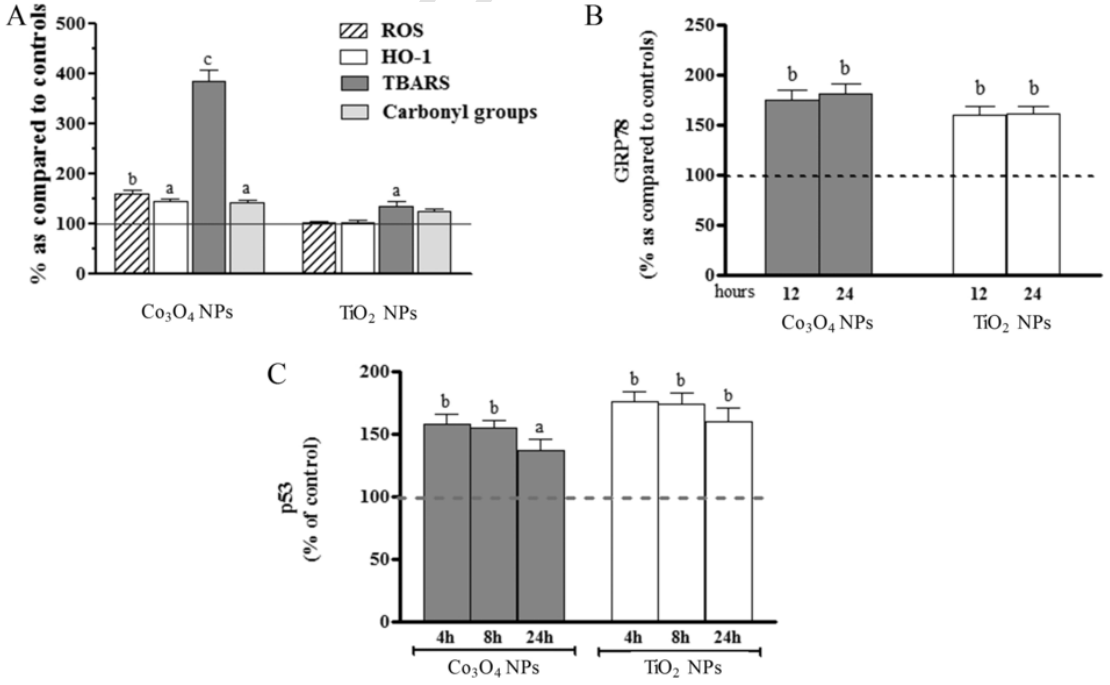

Fig. 6. (A) Oxidative stress during exposure of cells to NPs (50 μg/ml). Values are mean ± SD of three separate experiments, each carried out in triplicate and expressed as percentage of control. Significantly different from untreated control: [a]: $p < 0.05$; [b]: $p < 0.01$; [c]: $p < 0.001$. (B) Effects of NPs on endoplasmic reticulum. Significantly different from untreated control: [a]:$p < 0.05$; [b]: $p < 0.01$; [c]: $p < 0.001$. (C) Flow cytometry-based evaluation of p53 expression in A549 cells treated with NPs. Data are expressed as Mean (treated/control) ± SD. Significantly different from untreated control: [a]:$p < 0.05$; [b]: $p < 0.01$; [c]: $p < 0.001$.

molecules and release of inflammation mediators. Based on these findings, we propose here a model to study the effects of the same NPs on a pulmonary cell line. Cell line A549 cell line was chosen because it is widely used in toxicological studies due to its xenobiotic metabolic properties that are characteristic of normal human alveolar type 2 epithelial cells (Vulimiri et al., 2009). A recent study reported direct and oxidative DNA damage without any cytotoxic effect or increased cytokine release in A549 cells treated with Co_3O_4 NPs (Cavallo et al., 2015), while it has been recently demonstrated that TiO_2 NPs are not cytotoxic to human alveolar A549 cells (Moschini et al., 2013). Furthermore, modest viability reduction and moderate membrane damage at the concentration of 40 μg/ml were observed (Ursini et al., 2014). Therefore, the concentrations of NPs used in this study are consistent with literature. Although it is improbable that such an accumulation of NPs is present in "real life exposure", it should be noted that in in vivo studies with animals the accumulation of NPs in the lung is not homogeneous. Some metals (Ag, Zn) accumulate in spots of tens of μg/g (Baek et al., 2012; Smulders et al., 2015), and Ti in the range of 4–20 μg/g (Krystek et al., 2014). Given that the specific weight of pulmonary tissue is slightly above 1 g/ml at rest, local pulmonary exposure in the same order of magnitude is plausible.

Our aim was to further explore cellular alterations induced by TiO_2 NPs also in the absence of evident cellular cytotoxic effects, by using Co_3O_4 NPs as comparison term. Both NPs tend to aggregate both in water and in culture media, and therefore the interaction between relatively strongly bonded aggregates or soft agglomerates of NPs containing metals and live cells may be a key passage in justifying NP toxicity. A limitation of the study is that A549 cells were not grown at the air-liquid interface (ALI), an emerging cell culture practice where particles can maintain their intrinsic characteristics until they reach the cells, and the in vitro exposure mimics better the in vivo one. Studies on TiO_2 NPs support their ability to induce direct dose-dependent damage at the air–liquid interface on A549 cells (Steinritz et al., 2013). However, ALI needs further optimization and standardization (Latvala et al., 2016; Secondo et al., 2016), and we preferred to perform our experiments in the traditional but highly reproducible submerged culture, with the intention to contribute, in a near future, to standardize an ALI system to deal with pulmonary cells.

A first difference observed between these two NPs tested concerns the "corona". Based on literature reports, it is expected that NPs are covered by a protein corona upon application to a biological system or in a culture medium containing FBS (Lundqvist et al., 2008; Monopoli et al., 2011). The composition of this corona may have a major influence on the cellular uptake or cytotoxicity (Aggarwal et al., 2009; Monopoli et al., 2011). The amount of proteins bound to TiO_2 NPs was much higher than that of Co_3O_4 NPs, explainable by a difference in diameter/surface values and zeta potential. It is interesting to note an opposite effect of protein corona on the aggregation state in culture media: TiO_2 NPs form larger aggregates than Co_3O_4 NPs (Alinovi et al., 2015). These results should be cautiously interpreted, as no in-depth study on the composition of the corona has been performed here. It is evident that the composition was similar for the most abundant serum proteins, but we have no information about specific and less abundant proteins, which might have a role in NPs uptake. Further studies are therefore necessary in this field with these commercially available NPs.

The internalization of both NPs is rapid (Alinovi et al., 2015; Janer et al., 2014). However, a discrepancy is evident: the concentration of the absorbed Co was ten-time higher than Ti and this is not explainable in terms of a difference in the chemical composition and in the solubility of NPs (TiO_2 NPs were more soluble than Co_3O_4 NPs). On the other hand, flow cytometry showed a more significant modification of SSC in cells treated with TiO_2 NPs, explainable as a change the internal structure of the cell and its granulometry due to autophagy, which influences the SSC signal. Therefore, this may limit the use of flow cytometry to a unique qualitative assessment of NPs uptake. Given the possible toxicity of soluble Co^{3+} ions, some experiments about dissolution of Co were performed. The internal cellular solubility of Co increased its uptake from about 3.3 (SD: 0.1) ng/10^6 cells [cells only exposed to ions released by NPs in solution, estimated concentration 4.75 μM] to 23.6 (SD: 3.5) ng/10^6, like the nominal exposure to soluble Co was 34 μM [soluble intracellular Co fraction after 24 h-NP exposure at 50 μg/ml]. Since (a) no cytotoxic effects of Co salts were observed until to 100 μM, as also expected by literature (Horev-Azaria et al., 2011) and (b) the Co concentration in the pellet was three orders of magnitude higher that the soluble fraction, contrarily to other highly soluble Co NPs used in literature (Horev-Azaria et al., 2011), the observed effects must be prevalently due to Co_3O_4 in the NP form.

Our findings clearly demonstrate that even very high concentrations of NPs have few cytotoxic effects on A549 cells. However, Co_3O_4 NPs impaired cell metabolism in a concentration- and time-dependent manner. These observations are in agreement with other studies (Moschini et al., 2013; Prasad et al., 2013; Pujalte et al., 2011; Strobel et al., 2014). However, the internalization of both NPs reduced the proliferative capacity of the cells at late time, as observed in the clonogenic assay. Furthermore, both tested NPs elicited similar impact on endoplasmic reticulum, as suggested by some authors (Chen et al., 2014; Yu et al., 2015a). In line with other studies (Alarifi et al., 2013; Colognato et al., 2008; Papis et al., 2009), we found that Co_3O_4 NPs rapidly induced ROS and the formation of peroxidized products, contrarily to TiO_2 NPs (few modest effects only at 24 h-exposure). The decreased cell number after treatment with the NPs, given the absence of effects on apoptosis and necrosis markers, is probably due to an effect of NPs on cell cycle. Further experiments are in progress to shed light on the phenomenon.

Currently, attention is being paid to the relationship between NPs and autophagy (Kenzaoui et al., 2012; Mao et al., 2016; Nowak et al., 2014; Zhang et al., 2016). Autophagy might be considered a protective mechanism in cells. There are several forms of autophagy, but all involve the delivery of cell components to lysosomes in response to sub-lethal cell stress. Generalized high vacuolization of cells is an autophagy characteristic that is observed in cells exposed to the NPs. NP-mediated autophagy may be an adaptive cellular response, aiding in the degradation and clearance of nanomaterials, but may also cause harmful cellular dysfunction. Our observations on TiO_2 NPs are consistent with literature (Lopes et al., 2016). It has been recently observed that inhaled TiO_2 nanoparticles led to autophagic response in murine lung associated with ER swelling and mitochondrial disruption (Yu et al., 2015b). Importantly, autophagy may depend on the dispersity of NPs (Huang et al., 2015). Our results are in line with the tendency of TiO_2 NPs to form aggregates of hundreds of nm, increasing therefore the NP dispersity and activate autophagic mechanisms. Co_3O_4 NPs form lesser aggregates in culture media. This observation, together with the high Co intracellular accumulation, may indicate that aggregates of Co_3O_4 NPs may release a higher number of dispersed NPs as compared to TiO_2 NPs, and therefore aggregation and NP uptake may be competitive processes. This hypothesis is well sustained by TEM images (Fig. 1A–B): Co_3O_4 NPs were highly dispersed as compared to the aggregates observed for TiO_2 NPs. Therefore, autophagy may be differentially induced by NP aggregates of different dimensions. It has been recently demonstrated that TiO_2 NPs in podocytes induce autophagy with the activation of AMPK, and it protects cells from oxidative stress (Zhang et al., 2016). The link between autophagy and oxidative stress is present with other NPs (Petrache Voicu et al., 2015). However, in our experiments oxidative stress seems to be only marginally involved in the toxicity of TiO_2 NPs on A549 cells, independently from authopagy.

Autophagic response can be modulated by the expression of miRNAs. Several miRNAs have been identified as suppressors of factors

involved in different stages of autophagy while others have been shown to induce autophagy (Yu et al., 2012; Zheng et al., 2015). MiRNA-21 (hsa-miRNA-21) is up-regulated in all types of human cancer including lung carcinoma (Yang et al., 2014). It is involved in all cancer-related processes including tumorigenesis, progression and metastasis and its expression is associated with clinical-pathological factors and prognosis (Markou et al., 2008). Inhibition of miRNA-21 can induce cell cycle arrest, and increase chemosensitivity to anticancer agents (Papagiannakopoulos et al., 2008). MiRNA-21 plays a role also in autophagy (Liu et al., 2015; Seca et al., 2013), and its silencing enhances autophagic cell death (Gwak et al., 2012; Yu et al., 2016). Furthermore, miRNA-21 inhibition reduces proliferation, migration, and invasion of A549 cells (Yang et al., 2015). Importantly, miRNA-21 overexpression can inhibit autophagy, only partially mediated by the Akt/mTOR signaling pathway (Huang et al., 2016). Similar inhibitory activity is suggested for miRNA-30a: it was shown to inhibit Beclin-1 activity, thereby blocking autophagic vesicle nucleation and autophagy initiation (Yu et al., 2012; Zhu et al., 2009).

Recent studies revealed that also miRNA-155 can impact the autophagic cascade: an inverse correlation between the miRNA-155 levels and autophagic flux in human chondrocytes has been demonstrated (D'Adamo et al., 2016) and increased levels of miRNA-155 drastically suppress autophagy. On the contrary, other authors reported its pro-autophagy effects in human nasopharyngeal and cervical cancer cells (Wan et al., 2014). Interplays and feedback loops between these miRNA and the p53 pathway has been unveiled (Bouamar et al., 2015; Park et al., 2016). A fundamental factor controlling these processes involved in cellular response to noxa is the tumor suppressor p53, which primarily acts as a transcription factor (Ryan, 2011).

Only TiO_2 NPs were able to stimulate the autophagic pathway, which was accompanied by a reduced expression of miRNA-21 and miRNA-30a at all time-points tested (50 μg/ml), while it was transient with Co_3O_4 NPs. Interestingly, no significant differences between 24-h exposure to TiO_2 NPs and controls were observed when autophagy was blocked by 3-MA, indicating an inverse relationship between these miRNA expression and autophagy induction. Differently, miRNA-155 had the same time trend in both exposures, indicating that its expression is not related to autophagy induction. Cells react to particle exposure inducing an increase of miRNA-155 expression, as observed with other tumoral cell lines in response to chemotherapic agents. However, cells are not capable of detoxifying from NPs, that persist in the cytoplasm, justifying so the under-expression observed later.

In summary, both NPs caused in A549 cells similar effects on ER stress, and the most evident cytotoxic effects were observed for Co_3O_4 NPs at time exposure $\leq$ 72 h. The production of ROS was evident in Co_3O_4 NP, but only marginal in TiO_2 NP exposure. The oxidative stress caused by Co_3O_4 NPs can influence energy homeostasis and drive the cellular response and the ability to detoxify and to repair the resulting damage, thus preventing the induction of the autophagic pathway. TiO_2 NPs elicit autophagy accumulation in lung cells also under sub-toxic conditions. Defense mechanisms often save the cell but might trigger harmful late responses. Therefore, the modifications of organelles balance induced by TiO_2 NPs should not be underestimated, suggesting the potential of these NPs to elicit adverse effects over prolonged exposure conditions. Finally, we provided further evidences linking miRNAs under-expression and the induction of the autophagy pathway.

Conflict of interest

Matteo Goldoni is associate Editor of this journal. Other authors declare that there are no conflicts of interest.

Transparency document

The Transparency document associated with this article can be found, in online version.

Acknowledgements

This study was supported by the Ministry of Health, Italy Ricerca Finalizzata 2009 Grant: Integrated approach to evaluating the biological effects on lung, cardiovascular system and skin of occupational exposure to nanomaterials (NanO I-LuCaS). RF-2009-1472550.

Appendix A. Supplementary data

Supplementary data to this article can be found online at http://dx.doi.org/10.1016/j.tiv.2017.04.007.

References

Aggarwal, P., Hall, J.B., McLeland, C.B., Dobrovolskaia, M.A., McNeil, S.E., 2009. Nanoparticle interaction with plasma proteins as it relates to particle biodistribution, biocompatibility and therapeutic efficacy. Adv. Drug Deliv. Rev. 61, 428–437.

Alarifi, S., Ali, D., Suliman, Y.A.O., Ahamed, M., Siddiqui, M.A., Al-Khedhairy, A.A., 2013. Oxidative stress contributes to cobalt oxide nanoparticles-induced cytotoxicity and DNA damage in human hepatocarcinoma cells. Int. J. Nanomedicine 8, 189–199.

Alinovi, R., Goldoni, M., Pinelli, S., Campanini, M., Aliat, I., Bersani, D., Lottici, P.P., Iavicoli, S., Petyx, M., Mozzoni, P., Mutti, A., 2015. Oxidative and pro-inflammatory effects of cobalt and titanium oxide nanoparticles on aortic and venous endothelial cells. Toxicol. in Vitro 29, 426–437.

Baek, M., Chung, H.E., Yu, J., Lee, J.A., Kim, T.H., Oh, J.M., Lee, W.J., Paek, S.M., Lee, J.K., Jeong, J., Choy, J.H., Choi, S.J., 2012. Pharmacokinetics, tissue distribution, and excretion of zinc oxide nanoparticles. Int. J. Nanomedicine 7, 3081–3097.

Boffetta, P., Soutar, A., Cherrie, J.W., Granath, F., Andersen, A., Anttila, A., Blettner, M., Gaborieau, V., Klug, S.J., Langard, S., Luce, D., Merletti, F., Miller, B., Mirabelli, D., Pukkala, E., Adami, H.O., Weiderpass, E., 2004. Mortality among workers employed in the titanium dioxide production industry in Europe. Cancer Causes Control 15, 697–706.

Bouamar, H., Jiang, D.F., Wang, L., Lin, A.P., Ortega, M., Aguiar, R.C.T., 2015. MicroRNA 155 control of p53 activity is context dependent and mediated by Aicda and Socs1. Mol. Cell. Biol. 35, 1329–1340.

Cacchioli, A., Ravanetti, F., Alinovi, R., Pinelli, S., Rossi, F., Negri, M., Bedogni, E., Campanini, M., Galetti, M., Goldoni, M., Lagonegro, P., Alfieri, R., Bigi, F., Salviati, G., 2014. Cytocompatibility and cellular internalization mechanisms of SiC/SiO2 nanowires. Nano Lett. 14, 4368–4375.

Cavallo, D., Ciervo, A., Fresegna, A.M., Maiello, R., Tassone, P., Buresti, G., Casciardi, S., Iavicoli, S., Ursini, C.L., 2015. Investigation on cobalt-oxide nanoparticles cyto-genotoxicity and inflammatory response in two types of respiratory cells. J. Appl. Toxicol. 35, 1102–1113.

Chatterjee, S., Sarkar, S., Bhattacharya, S., 2014. Toxic metals and autophagy. Chem. Res. Toxicol. 27, 1887–1900.

Chen, R., Huo, L.L., Shi, X.F., Bai, R., Zhang, Z.J., Zhao, Y.L., Chang, Y.Z., Chen, C.Y., 2014. Endoplasmic reticulum stress induced by zinc oxide nanoparticles is an earlier biomarker for nanotoxicological evaluation. ACS Nano 8, 2562–2574.

Colognato, R., Bonelli, A., Ponti, J., Farina, M., Bergamaschi, E., Sabbioni, E., Migliore, L., 2008. Comparative genotoxicity of cobalt nanoparticles and ions on human peripheral leukocytes in vitro. Mutagenesis 23, 377–382.

Crosera, M., Prodi, A., Mauro, M., Pelin, M., Florio, C., Bellomo, F., Adami, G., Apostoli, P., De Palma, G., Bovenzi, M., Campanini, M., Filon, F.L., 2015. Titanium dioxide nanoparticle penetration into the skin and effects on HaCaT cells. Int. J. Environ. Res. Public Health 12, 9282–9297.

D'Adamo, S., Alvarez-Garcia, O., Muramatsu, Y., Flamigni, F., Lotz, M.K., 2016. MicroRNA-155 suppresses autophagy in chondrocytes by modulating expression of autophagy proteins. Osteoarthr. Cartil. 24, 1082–1091.

EPA, 2009. Final Nanomaterial Research Strategy (NRS). US Environmental Protection Agency, Washington, USA.

Frankel, L.B., Lund, A.H., 2012. MicroRNA regulation of autophagy. Carcinogenesis 33, 2018–2025.

Gwak, H.S., Kim, T.H., Jo, G.H., Kim, Y.J., Kwak, H.J., Kim, J.H., Yin, J., Yoo, H., Lee, S.H., Park, J.B., 2012. Silencing of MicroRNA-21 confers radio-sensitivity through inhibition of the PI3K/AKT pathway and enhancing autophagy in malignant glioma cell lines. PLoS One 7, e47449.

Han, S.G., Newsome, B., Hennig, B., 2013. Titanium dioxide nanoparticles increase inflammatory responses in vascular endothelial cells. Toxicology 306, 1–8.

Horev-Azaria, L., Kirkpatrick, C.J., Korenstein, R., Marche, P.N., Maimon, O., Ponti, J., Romano, R., Rossi, F., Golla-Schindler, U., Sommer, D., Uboldi, C., Unger, R.E., Villiers, C., 2011. Predictive toxicology of cobalt nanoparticles and ions: comparative in

vitro study of different cellular models using methods of knowledge discovery from data. Toxicol. Sci. 122, 489–501.
Huang, D.T., Zhou, H.L., Gao, J.H., 2015. Nanoparticles modulate autophagic effect in a dispersity-dependent manner. Sci. Rep. 5, 14361.
Huang, Z., Wu, S., Kong, F., Cai, X., Ye, B., Shan, P., Huang, W., 2016. MicroRNA-21 protects against cardiac hypoxia/reoxygenation injury by inhibiting excessive autophagy in H9c2 cells via the Akt/mTOR pathway. J. Cell. Mol. Med. (In Press).
IARC, 2010. Carbon black, titanium dioxide, and talc. IARC Monogr. Eval. Carcinog. Risks Hum. 1–413.
Janer, G., del Molino, E.M., Fernandez-Rosas, E., Fernandez, A., Vazquez-Campos, S., 2014. Cell uptake and oral absorption of titanium dioxide nanoparticles. Toxicol. Lett. 228, 103–110.
Jugan, M.L., Barillet, S., Simon-Deckers, A., Herlin-Boime, N., Sauvaigo, S., Douki, T., Carriere, M., 2012. Titanium dioxide nanoparticles exhibit genotoxicity and impair DNA repair activity in A549 cells. Nanotoxicology 6, 501–513.
Karlsson, H.L., Cronholm, P., Gustafsson, J., Moller, L., 2008. Copper oxide nanoparticles are highly toxic: a comparison between metal oxide nanoparticles and carbon nanotubes. Chem. Res. Toxicol. 21, 1726–1732.
Kenzaoui, B.H., Bernasconi, C.C., Guney-Ayra, S., Juillerat-Jeanneret, L., 2012. Induction of oxidative stress, lysosome activation and autophagy by nanoparticles in human brain-derived endothelial cells. Biochem. J. 441, 813–821.
Krystek, P., Tentschert, J., Nia, Y., Trouiller, B., Noel, L., Goetz, M.E., Papin, A., Luch, A., Guerin, T., de Jong, W.H., 2014. Method development and inter-laboratory comparison about the determination of titanium from titanium dioxide nanoparticles in tissues by inductively coupled plasma mass spectrometry. Anal. Bioanal. Chem. 406, 3853–3861.
Larese Filon, F., Crosera, M., Timeus, E., Adami, G., Bovenzi, M., Ponti, J., Maina, G., 2013. Human skin penetration of cobalt nanoparticles through intact and damaged skin. Toxicol. in Vitro 27, 121–127.
Latvala, S., Hedberg, J., Moller, L., Odnevall Wallinder, I., Karlsson, H.L., Elihn, K., 2016. Optimization of an air-liquid interface exposure system for assessing toxicity of airborne nanoparticles. J. Appl. Toxicol. 36, 1294–1301.
Lindberg, H.K., Falck, G.C.M., Catalan, J., Koivisto, A.J., Suhonen, S., Jarventaus, H., Rossi, E.M., Nykasenoja, H., Peltonen, Y., Moreno, C., Alenius, H., Tuomi, T., Savolainen, K.M., Norppa, H., 2012. Genotoxicity of inhaled nanosized TiO2 in mice. Mutat. Res. Genet. Toxicol. Environ. Mutagen. 745, 58–64.
Liu, X.J., Hong, Q., Wang, Z., Yu, Y.Y., Zou, X., Xu, L.H., 2015. MiR-21 inhibits autophagy by targeting Rab11a in renal ischemia/reperfusion. Exp. Cell Res. 338, 64–69.
Livak, K.J., Schmittgen, T.D., 2001. Analysis of relative gene expression data using real-time quantitative PCR and the 2(T)(− Delta Delta C) method. Methods 25, 402–408.
Lopes, V.R., Loitto, V., Audinot, J.N., Bayat, N., Gutleb, A.C., Cristobal, S., 2016. Dose-dependent autophagic effect of titanium dioxide nanoparticles in human HaCaT cells at non-cytotoxic levels. J. Nanobiotech. 14, 22.
Lundqvist, M., Stigler, J., Elia, G., Lynch, I., Cedervall, T., Dawson, K.A., 2008. Nanoparticle size and surface properties determine the protein corona with possible implications for biological impacts. Proc. Natl. Acad. Sci. U. S. A. 105, 14265–14270.
Mao, B.H., Tsai, J.C., Chen, C.W., Yan, S.J., Wang, Y.J., 2016. Mechanisms of silver nanoparticle-induced toxicity and important role of autophagy. Nanotoxicology 10, 1021–1040.
Markou, A., Tsaroucha, E.G., Kaklamanis, L., Fotinou, M., Georgoulias, V., Lianidou, E.S., 2008. Prognostic value of mature microRNA-21 and microRNA-205 overexpression in non-small cell lung cancer by quantitative real-time RT-PCR. Clin. Chem. 54, 1696–1704.
Monopoli, M.P., Walczyk, D., Campbell, A., Elia, G., Lynch, I., Bombelli, F.B., Dawson, K.A., 2011. Physical-chemical aspects of protein corona: relevance to in vitro and in vivo biological impacts of nanoparticles. J. Am. Chem. Soc. 133, 2525–2534.
Montiel-Davalos, A., Luis Ventura-Gallegos, J., Alfaro-Moreno, E., Soria-Castro, E., Garcia-Latorre, E., Gerardo Cabanas-Moreno, J., del Pilar Ramos-Godinez, M., Lopez-Marure, R., 2012. TiO2 nanoparticles induce dysfunction and activation of human endothelial cells. Chem. Res. Toxicol. 25, 920–930.
Moschini, E., Gualtieri, M., Colombo, M., Fascio, U., Camatini, M., Mantecca, P., 2013. The modality of cell-particle interactions drives the toxicity of nanosized CuO and TiO2 in human alveolar epithelial cells. Toxicol. Lett. 222, 102–116.
NIOSH, 2011. Current intelligence bulletin 63. In: Occupational Exposure to Titanium Dioxide. National Institute for Occupational Safety and Health, Atlanta, USA.
Nowak, J.S., Mehn, D., Nativo, P., Garcia, C.P., Gioria, S., Ojea-Jimenez, I., Gilliland, D., Rossi, F., 2014. Silica nanoparticle uptake induces survival mechanism in A549 cells by the activation of autophagy but not apoptosis. Toxicol. Lett. 224, 84–92.
Papagiannakopoulos, T., Shapiro, A., Kosik, K.S., 2008. MicroRNA-21 targets a network of key tumor-suppressive pathways in glioblastoma cells. Cancer Res. 68, 8164–8172.
Papis, E., Rossi, F., Raspanti, M., Dalle-Donne, I., Colombo, G., Milzani, A., Bernardini, G., Gornati, R., 2009. Engineered cobalt oxide nanoparticles readily enter cells. Toxicol. Lett. 189, 253–259.
Park, D., Kim, H., Kim, Y., Jeoung, D., 2016. miR-30a regulates the expression of CAGE and p53 and regulates the response to anti-cancer drugs. Mol. Cell 39, 299–309.
Petrache Voicu, S.N., Dinu, D., Sima, C., Hermenean, A., Ardelean, A., Codrici, E., Stan, M.S., Zarnescu, O., Dinischiotu, A., 2015. Silica nanoparticles induce oxidative stress and autophagy but not apoptosis in the MRC-5 cell line. Int. J. Mol. Sci. 16, 29398–29416.
Prasad, R.Y., Wallace, K., Daniel, K.M., Tennant, A.H., Zucker, R.M., Strickland, J., Dreher, K., Kligerman, A.D., Blackman, C.F., DeMarini, D.M., 2013. Effect of treatment media on the agglomeration of titanium dioxide nanoparticles: impact on genotoxicity, cellular interaction, and cell cycle. ACS Nano 7, 1929–1942.
Pujalte, I., Passagne, I., Brouillaud, B., Treguer, M., Durand, E., Ohayon-Courtes, C., L'Azou, B., 2011. Cytotoxicity and oxidative stress induced by different metallic nanoparticles on human kidney cells. Part. Fibre Toxicol. 8, 10.
Ravanetti, F., Borghetti, P., De Angelis, E., Chiesa, R., Martini, F.M., Gabbi, C., Cacchioli, A., 2010. In vitro cellular response and in vivo primary osteointegration of electrochemically modified titanium. Acta Biomater. 6, 1014–1024.
Ryan, K.M., 2011. p53 and autophagy in cancer: guardian of the genome meets guardian of the proteome. Eur. J. Cancer 47, 44–50.
Sager, T.M., Kommineni, C., Castranova, V., 2008. Pulmonary response to intratracheal instillation of ultrafine versus fine titanium dioxide: role of particle surface area. Part. Fibre Toxicol. 5, 17.
Seca, H., Lima, R.T., Lopes-Rodrigues, V., Guimaraes, J.E., Almeida, G.M., Vasconcelos, M.H., 2013. Targeting miR-21 induces autophagy and chemosensitivity of leukemia cells. Curr. Drug Targets 14, 1135–1143.
Secondo, L.E., Liu, N.J., Lewinski, N.A., 2016. Methodological considerations when conducting in vitro, air-liquid interface exposures to engineered nanoparticle aerosols. Crit. Rev. Toxicol. 1–38.
Shi, H.B., Magaye, R., Castranova, V., Zhao, J.S., 2013. Titanium dioxide nanoparticles: a review of current toxicological data. Part. Fibre Toxicol. 10, 15.
Skocaj, M., Filipic, M., Petkovic, J., Novak, S., 2011. Titanium dioxide in our everyday life; is it safe?. Radiol. Oncol. 45, 227–247.
Smulders, S., Larue, C., Sarret, G., Castillo-Michel, H., Vanoirbeek, J., Hoet, P.H., 2015. Lung distribution, quantification, co-localization and speciation of silver nanoparticles after lung exposure in mice. Toxicol. Lett. 238, 1–6.
Spigoni, V., Cito, M., Alinovi, R., Pinelli, S., Passeri, G., Zavaroni, I., Goldoni, M., Campanini, M., Aliatis, I., Mutti, A., Bonadonna, R.C., Dei Cas, A., 2015. Effects of TiO(2) and Co(3)O(4) nanoparticles on circulating angiogenic cells. PLoS One 10, e0119310.
Srivastava, R.K., Rahman, Q., Kashyap, M.P., Singh, A.K., Jain, G., Jahan, S., Lohani, M., Lantow, M., Pant, A.B., 2013. Nano-titanium dioxide induces genotoxicity and apoptosis in human lung cancer cell line, A549. Hum. Exp. Toxicol. 32, 153–166.
Steinritz, D., Mohle, N., Pohl, C., Papritz, M., Stenger, B., Schmidt, A., Kirkpatrick, C.J., Thiermann, H., Vogel, R., Hoffmann, S., Aufderheide, M., 2013. Use of the Cultex(R) radial flow system as an in vitro exposure method to assess acute pulmonary toxicity of fine dusts and nanoparticles with special focus on the intra- and inter-laboratory reproducibility. Chem. Biol. Interact. 206, 479–490.
Stern, S.T., Adiseshaiah, P.P., Crist, R.M., 2012. Autophagy and lysosomal dysfunction as emerging mechanisms of nanomaterial toxicity. Part. Fibre Toxicol. 9, 20.
Strobel, C., Torrano, A., Herrman, R., Malissek, M., Brauchle, C., Reller, A., Treuel, L., Hilger, I., 2014. Effects of the physicochemical properties of titanium dioxide nanoparticles, commonly used as sun protection agents, on microvascular endothelial cells. J. Nanopart. Res. 16, 2130.
Sycheva, L.P., Zhurkov, V.S., Iurchenko, V.V., Daugel-Dauge, N.O., Kovalenko, M.A., Krivtsova, E.K., Durnev, A.D., 2011. Investigation of genotoxic and cytotoxic effects of micro- and nanosized titanium dioxide in six organs of mice in vivo. Mutat. Res. Genet. Toxicol. Environ. Mutagen. 726, 8–14.
Titma, T., Shimmo, R., Siigur, J., Kahru, A., 2016. Toxicity of antimony, copper, cobalt, manganese, titanium and zinc oxide nanoparticles for the alveolar and intestinal epithelial barrier cells in vitro. Cytotechnology 68, 2363–2377.
Ursini, C.L., Cavallo, D., Fresegna, A.M., Ciervo, A., Maiello, R., Tassone, P., Buresti, G., Casciardi, S., Iavicoli, S., 2014. Evaluation of cytotoxic, genotoxic and inflammatory response in human alveolar and bronchial epithelial cells exposed to titanium dioxide nanoparticles. J. Appl. Toxicol. 34, 1209–1219.
Vulimiri, S.V., Misra, M., Hamm, J.T., Mitchell, M., Berger, A., 2009. Effects of mainstream cigarette smoke on the global metabolome of human lung epithelial cells. Chem. Res. Toxicol. 22, 492–503.
Wan, G., Xie, W.D., Liu, Z.Y., Xu, W., Lao, Y.Z., Huang, N.N., Cui, K., Liao, M.J., He, J., Jiang, Y.Y., Yang, B.B., Xu, H.X., Xu, N.H., Zhang, Y.U., 2014. Hypoxia-induced MIR155 is a potent autophagy inducer by targeting multiple players in the MTOR pathway. Autophagy 10, 70–79.
Yang, X., Guo, Y., Du, Y., Yang, J., Li, S., Liu, S., Li, K., Zhang, D., 2014. Serum microRNA-21 as a diagnostic marker for lung carcinoma: a systematic review and meta-analysis. PLoS One 9, e97460.
Yang, Y., Meng, H., Peng, Q., Yang, X., Gan, R., Zhao, L., Chen, Z., Lu, J., Meng, Q.H., 2015. Downregulation of microRNA-21 expression restrains non-small cell lung cancer cell proliferation and migration through upregulation of programmed cell death 4. Cancer Gene Ther. 22, 23–29.
Yao, D.H., Wang, P.Q., Zhang, J., Fu, L.L., Ouyang, L., Wang, J.H., 2016. Deconvoluting the relationships between autophagy and metastasis for potential cancer therapy. Apoptosis 21, 683–698.
Yu, Y., Cao, L.Z., Yang, L.C., Kang, R., Lotze, M., Tang, D.L., 2012. microRNA 30A promotes autophagy in response to cancer therapy. Autophagy 8, 853–855.
Yu, K.N., Chang, S.H., Park, S.J., Lim, J., Lee, J., Yoon, T.J., Kim, J.S., Cho, M.H., 2015. Titanium dioxide nanoparticles induce endoplasmic reticulum stress-mediated autophagic cell death via mitochondria-associated endoplasmic reticulum membrane disruption in normal lung cells. PLoS One 10, e0131208.
Yu, K.N., Sung, J.H., Lee, S., Kim, J.E., Kim, S., Cho, W.Y., Lee, A.Y., Park, S.J., Lim, J., Park, C., Chae, C., Lee, J.K., Lee, J., Kim, J.S., Cho, M.H., 2015. Inhalation of titanium dioxide induces endoplasmic reticulum stress-mediated autophagy and inflammation in mice. Food Chem. Toxicol. 85, 106–113.
Yu, X.F., Li, R.L., Shi, W.N., Jiang, T., Wang, Y.F., Li, C., Qu, X.J., 2016. Silencing of MicroRNA-21 confers the sensitivity to tamoxifen and fulvestrant by enhancing au-

tophagic cell death through inhibition of the PI3K-AKT-mTOR pathway in breast cancer cells. Biomed. Pharmacother. 77, 37–44.
Zhang, X.C., Li, W., Yang, Z., 2015. Toxicology of nanosized titanium dioxide: an update. Arch. Toxicol. 89, 2207–2217.
Zhang, X., Yin, H., Li, Z., Zhang, T., Yang, Z., 2016. Nano-TiO2 induces autophagy to protect against cell death through antioxidative mechanism in podocytes. Cell Biol. Toxicol. 32, 513–527.
Zheng, B., Zhu, H., Gu, D.H., Pan, X.D., Qian, L., Xue, B.X., Yang, D.R., Zhou, J.D., Shan, Y.X., 2015. MiRNA-30a-mediated autophagy inhibition sensitizes renal cell carcinoma cells to sorafenib. Biochem. Biophys. Res. Commun. 459, 234–239.
Zhu, H., Wu, H., Liu, X.P., Li, B.A., Chen, Y., Ren, X.C., Liu, C.G., Yang, J.M., 2009. Regulation of autophagy by a beclin 1-targeted microRNA, miR-30a, in cancer cells. Autophagy 5, 816–823.